Available online at www.sciencedirect.com

SCIENCE DIRECT

Virology 342 (2005) 215 – 227

VIROLOGY

www.elsevier.com/locate/yviro

Influenza virus assembly and budding in raft-derived microdomains: A quantitative analysis of the surface distribution of HA, NA and M2 proteins

George P. Leser [a], Robert A. Lamb [a,b,*]

[a] Department of Biochemistry, Molecular Biology and Cell Biology, Northwestern University, 2205 Tech Drive, Evanston, IL 60208-3500, USA
[b] Howard Hughes Medical Institute, Northwestern University, Evanston, IL 60208-3500, USA

Received 29 June 2005; returned to author for revision 2 August 2005; accepted 20 September 2005
Available online 24 October 2005

Abstract

Influenza virus hemagglutinin (HA) and neuraminidase (NA) are known to associate with lipid rafts, membrane microdomains comprised of densely packed cholesterol and sphingolipids. These specialized membrane regions are believed to be involved in the budding of many enveloped viruses including influenza virus. Quantitative analysis of HA distribution on the surface of virus-infected cells by immunogold staining shows an organization into clusters that grow in size as the expression level of HA increases with time post-infection (p.i.) (~325–500 nm at 4 h p.i. and ~425–600 nm at 6 h p.i.). These HA-containing clusters are likely derived from lipid rafts as they contain a high density of the raft marker ganglioside GM1 and are dependent upon the presence of cholesterol. The clustering of HA is an intrinsic property of the HA protein and occurs in the absence of expression of other viral proteins. NA is also found sequestered within the same microdomains as HA, whereas the M2 ion channel protein does not concentrate within the raft-like microdomains. Quantification of the distribution of surface expressed HA by examining serial sections of virus-infected cells suggests that the HA-containing microdomains give rise to regions of influenza assembly and budding.

Keywords: Lipid microdomains; Influenza virus; Budding; Virus assembly; Hemagglutinin; Neuraminidase

Introduction

The lipids of the plasma membrane are distributed non-randomly and can self-associate and organize into a liquid ordered phase, which imparts lateral organization to model and cellular membranes (Ahmed et al., 1997; Rietveld and Simons, 1998; Schroeder et al., 1994). Sphingolipids and cholesterol contribute to cellular membrane organization by packing densely to form domains in the plasma membrane commonly called lipid rafts or detergent-resistant membranes (DRMs). The ganglioside GM1 is enriched in these lipid microdomains and is a useful marker for lipid rafts as it binds to the pentavalent B subunit of cholera toxin (Parton, 1994). The formation and structural integrity of these microdomains are dependent upon the presence of cholesterol, and the microdomains can be disrupted by depletion of cellular cholesterol (Carrasco et al., 2004; Keller and Simons, 1998; Varma and Mayor, 1998). Size estimates for rafts in the cellular plasma membrane vary from <5 nm to ~700 nm, and the size appears to be dependent on the method of analysis; however, a size of <100 nm is commonly cited (Pralle et al., 2000; Sharma et al., 2004; Varma and Mayor, 1998). It has been estimated that as much as ~50% of the cellular membrane exists as lipid rafts suggesting that there are small densely packed discrete structures that are beyond the resolving power of the light microscope. The ability to fractionate biochemically lipid rafts, using relatively low concentrations of non-ionic detergent (frequently Triton X-100) at low temperature (Brown and Rose, 1992; Chamberlain, 2004; Hooper, 1999; Schroeder et al., 1994; Simons and Ikonen, 1997) has given insight into their lipid and protein composition. Raft-affiliated proteins after detergent extraction float in sucrose gradients due to their continued association with raft lipids. Many proteins have demonstrated affinities for lipid rafts including GPI-anchored proteins (Brown and Rose, 1992; Rodgers et al., 1994), Src-

* Corresponding author. Department of Biochemistry, Molecular Biology and Cell Biology, Northwestern University, 2205 Tech Drive, Evanston, IL 60208-3500, USA. Fax: +1 847 491 2467.
E-mail address: ralamb@northwestern.edu (R.A. Lamb).

0042-6822/$ - see front matter © 2005 Elsevier Inc. All rights reserved.
doi:10.1016/j.virol.2005.09.049

family kinases (Robbins et al., 1995; Rodgers et al., 1994) and some transmembrane proteins including influenza virus hemagglutinin (HA) and neuraminidase (NA) (Barman and Nayak, 2000; Scheiffele et al., 1997; Zhang et al., 2000).

Rafts are thought to function as sites for the selective concentration of proteins, acting as platforms enabling a sufficient quantity of protein to accumulate to enable their function or to promote specific protein–protein interactions. Rafts are also thought to play roles in apical sorting in polarized cells (Keller and Simons, 1998), cell migration (Gomez-Mouton et al., 2001), IgE signaling (Sheets et al., 1999), T cell activation (Langlet et al., 2000), Ras signaling (Prior et al., 2001; Roy et al., 1999), PIP_2 signaling (Laux et al., 2000), and rafts have a role in the assembly of many enveloped viruses (Suomalainen, 2002). However, the role rafts play in cellular processes, or even their existence, is not universally agreed upon (Glebov and Nichols, 2004; Kenworthy et al., 2000; Munro, 2003).

Early studies of influenza virus budding showed that influenza virus appeared to assemble at discrete patches on the cell membrane (Compans and Dimmock, 1969; Morgan et al., 1961). It is now thought these patches are "raft-like" microdomains (Scheiffele et al., 1999; Takeda et al., 2003; Zhang et al., 2000). Several other enveloped viruses also use raft-like domains as platforms for virus assembly, e.g., HIV (Lindwasser and Resh, 2001; Nguyen and Hildreth, 2000; Ono and Freed, 2001), Ebola and Marburg viruses (Bavari et al., 2002) and measles virus (Vincent et al., 2000) (reviewed in (Suomalainen, 2002)). It is thought that viruses use rafts as sites of nucleation of viral components through interactions with host factors or interactions with other virally expressed proteins concentrated within these microdomains. For influenza virus, HA and NA concentrate in lipid microdomains (Barman and Nayak, 2000; Scheiffele et al., 1997; Zhang et al., 2000) and amino acid residues in the transmembrane domain of both HA and NA have been found to be important for raft association. However, it is not known if these amino acids interact with lipids of the plasma membrane directly or if the interaction is indirect involving other cellular components. The amino acids of the transmembrane domain that would be in a position to interact with the lipids of the outer membrane leaflet are of primary importance in mediating raft association of HA (Lin et al., 1998; Scheiffele et al., 1997; Takeda et al., 2003; Zhang et al., 2000). The evidence for a role for lipid rafts in influenza assembly and budding is strongly supported by an analysis of the lipid components of the influenza viral envelope that shows a composition similar to that of a Triton X-100 resistant membrane fraction (Scheiffele et al., 1999; Zhang et al., 2000). The generally accepted size range for lipid rafts is smaller than the diameters of many viruses that use rafts as platforms from which to bud. Thus, for influenza virus, the HA-containing rafts must be organized in some manner on the cell surface to provide a sufficient quantity of HA to support virus assembly.

To investigate the assembly process of influenza virus at the plasma membrane, we used a method of analytical immunoelectron microscopy (Brown and Lyles, 2003a; Philimonenko et al., 2000; Ripley, 1979) to examine the lateral organization of the viral integral membrane proteins HA, NA and the M2 ion channel on the cell surface. The data show that HA and NA but not M2 protein concentrate in "raft-like" structures that contain the ganglioside GM1. The structures are ~325–500 nm in diameter at 4 h p.i. and grow in size to become the site of viral budding. The site of budding (ranging in diameter from ~2 to 5 μm or more) has been termed the viral budozone (Schmitt and Lamb, 2004).

Results

We conducted a study using quantitative immunogold electron microscopy to examine the plasma membrane distribution of the influenza virus integral membrane proteins HA, NA and M2. As lipid rafts are dynamic structures, observations by microscopy could be influenced by the method chosen for analysis. Electron microscopy requires the use of fixed samples and electron dense markers. To minimize inter-domain traffic and to permit binding of bivalent antibodies and pentavalent subunit B of cholera toxin (CTB) with minimal patching of their target molecules, cells were incubated at 4 °C and immunogold labeled prior to fixation to maximize the sensitivity of CTB staining of GM1 and to avoid deleterious effects of fixation on antigen retention. The use of a stronger fixative/cross-linker, of 4% formaldehyde/0.2% glutaraldehyde at 4 °C, had no effect on the distribution of HA or GM1 in the membrane, indicating the milder fixation condition did not permit protein movement. Furthermore, the observation that raft-associated wild-type HA and mutant non-raft associated HA segregate very differently in the plasma membrane (Takeda et al., 2003) provides additional validation of the procedures used.

The distribution of influenza virus HA at the cell surface of virus-infected MDCK cells and CV1 cells at 6 h p.i. was analyzed. HA was detected using 15-nm gold particles (Fig. 1A), and the lipid raft marker GM1 was detected using CTB-linked to 6-nm gold particles (Fig. 1A and see below). The distribution of HA-specific 15-nm gold particles was quantified on non-budding regions of randomly selected membrane profiles using the methodological approaches of Ripley (1979), Philimonenko et al. (2000) and Brown and Lyles (2003a, 2003b, 2005). The areas of gold staining are thought to be the regions of plasma membrane that become the area of active virus budding (see below). In Fig. 1B, the *y*-intercept of the portion of the data having a slope of 0 represents the general average density of gold-labeled HA on the plasma membrane. The region of the plot with a negative slope is indicative of HA being organized into a membrane microdomain, a perpendicular line intersecting the *x*-axis from the point of slope break indicates the average diameter of the microdomain. MDCK cells had a higher average membrane density of HA (0.16 particles/20 nm), as compared to CV1 cells (0.04 particles/20 nm) (Fig. 1B). The 5- to 20-fold higher density of HA in MDCK cells than CV1 cells was confirmed by both flow cytometry and biotinylation of surface-labeled HA (data not shown). The average diameter of HA microdomains on the surface of MDCK cells was determined to be approximately ~425–600 nm, whereas for CV1 cells, the average diameter of HA microdomains was ~275–400 nm.

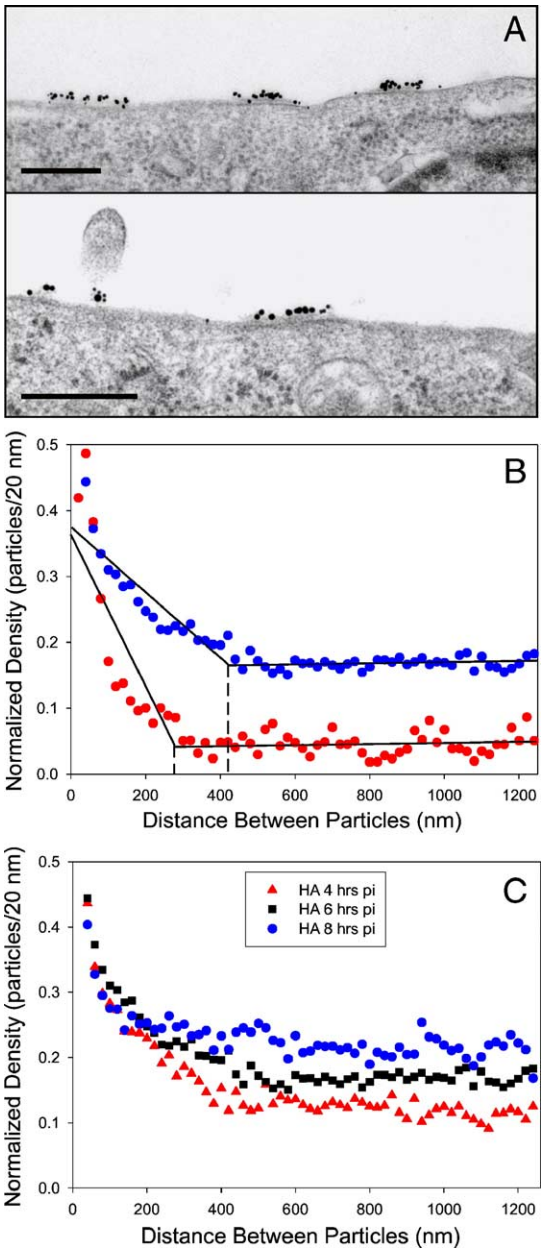

Fig. 1. The distribution of influenza virus HA on the surface of virus-infected cells. (A) Two examples of MDCK cells infected with influenza virus and, after 6 h p.i., stained with CTB conjugated to 6-nm gold particles and goat-anti-HA anti-serum followed by donkey anti-goat antibodies conjugated to 15-nm gold. Cells were infiltrated and embedded, thin sectioned and stained for electron microscopy (Scale bar = 0.5 μm). (B) The density and distribution of HA were determined from intervals between pairs of gold particles along the length of the plasma membrane in non-budding regions of either MDCK cells (blue) or CV1 cells (red) and analyzed according to the method of Brown and Lyles (2003a). For each cell line, 24 random profiles of separate cells were used for the analysis. (C) The density and distribution of HA on the surface of influenza virus-infected MDCK cells were determined by measuring ~30 cell profiles for each time point at 4 h (red), 6 h (black) or 8 h (blue) post-infection.

With increasing time of influenza virus infection, the diameters of the regions of clustered raft-associated HA increased, and concomitantly, the level of surface expression of HA also increased. In Fig. 1C, the distribution of HA staining on the surface of MDCK cells at 4, 6 and 8 h p.i. is shown, and it was observed that at increasing times p.i., the average expression level of HA on the cell surface increased, as illustrated by the shift upwards in the *y*-intercept of the region of the plot possessing a 0 slope. The average diameter of HA clusters after 4 h p.i. was ~325–500 nm and at 6 h p.i. was ~425–600 nm. At 8 h p.i., the distribution of HA over distance intervals of 20–460 nm is best described as a curved line, suggesting domains of multiple or varying sizes. Although quantification of HA distribution at 2 h p.i. was attempted, the level of HA labeling was too low to quantify, consisting of 21 gold particles spread over 130-μm of plasma membrane.

HA clusters contain the raft marker GM1 and likely represent a coalescence of rafts

The ganglioside GM1 has been characterized previously as a marker for lipid rafts (Parton, 1994). Pentavalent CTB has been used to stain specifically GM1 in the plasma membrane (Parton, 1994), and here, CTB conjugated to 6-nm gold particles was used to stain influenza virus-infected MDCK cells (Fig. 1A). To minimize any possible steric hindrance from bound antibodies, thereby resulting in a less accurate representation of the distribution of GM1, cells were stained with CTB gold prior to reaction with HA-specific serum. Despite these precautions, most of the HA-associated CTB staining was confined to the periphery of HA clusters or in areas within microdomains where HA staining was less dense. This is likely due to the highly packed nature of these clusters: when viewed unstained, the clusters frequently appear as densely packed with upright bristles. The distribution of CTB gold after 2 h p.i. (Fig. 2A) was different from that seen after 4 h p.i. (Fig. 2B). At 2 h p.i., very little HA expression on the cell surface was observed, and GM1 was distributed in uniform size microdomains with a diameter of ~125–200 nm (Fig. 2A). At 4 h p.i., the average membrane density of GM1 was similar to that at 2 h p.i. However, the analysis of CTB gold staining at 4 h p.i. indicated two changes in slope, suggesting microdomains of two distinct sizes with diameters of about ~75–125 nm and ~225–350 nm. At 4 h p.i., a portion of the GM1 co-localizes with HA in microdomains larger than those solely containing GM1. Two size populations of microdomains can be explained by a fraction of GM1 residing in non-HA-containing rafts, while a portion of GM1 is found in HA-containing raft clusters. The measured diameter of the larger GM1-containing microdomains did not have the same size as the HA clusters measured at 4 h p.i. and is likely due to the above discussed accessibility constraints restricting most of the HA-associated CTB gold staining. A comparison of the GM1 distribution after 2, 4, 6 and 8 h p.i. is shown in Fig. 2C. As expected, the average membrane concentration of GM1 remained generally similar at all times p.i. The distinction between the two populations of GM1-containing microdomains was present but less clearly defined after 6 h p.i. and was not detectable at 8 h p.i. when the expression of HA on the cell surface was greater. A higher density of HA in microdomains at later times p.i. made the efficient staining of any resident GM1 increasingly difficult.

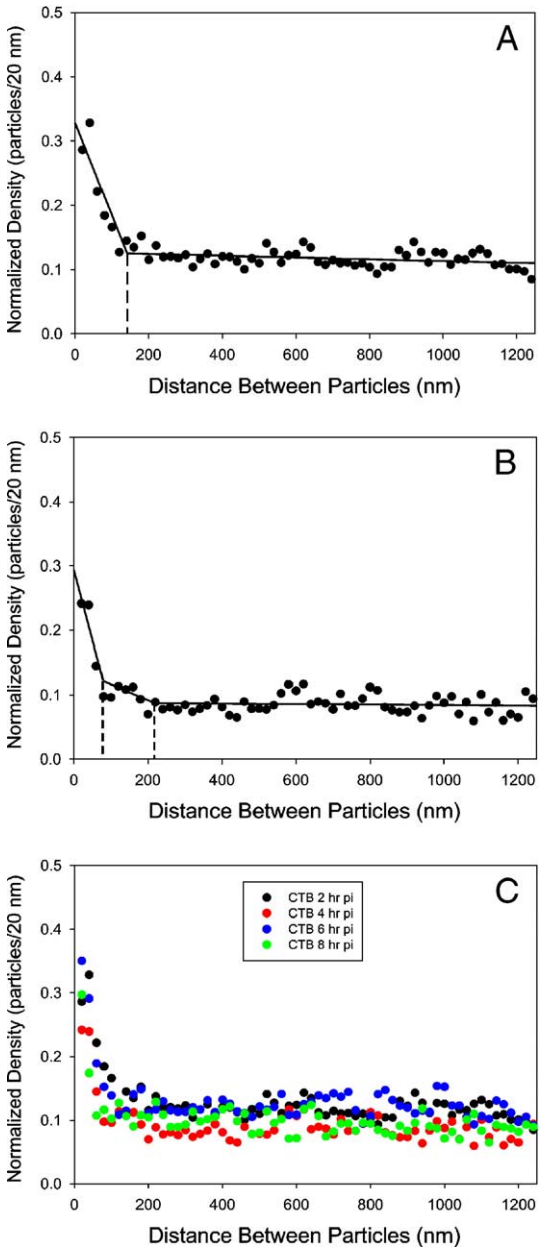

Fig. 2. The surface distribution of ganglioside GM1 is altered on influenza virus infection. Influenza virus-infected MDCK cells were stained with CTB conjugated to 6-nm gold particles and goat-anti-HA anti-serum, followed by donkey anti-goat antibodies conjugated to 15-nm gold. (A) CTB gold distribution on virus-infected MDCK cells at 2 h p.i. was determined from 29 cell profiles. (B) CTB gold distribution on influenza virus-infected MDCK cells at 4 h p.i. The analysis was derived from 28 cell profiles. (C) The distribution of GM1 as visualized by CTB gold staining of influenza virus-infected MDCK cells at 2 h (black), 4 h (red), 6 h (blue) and 8 h (green) p.i.

To determine if the HA-containing membrane domains are enriched in GM1 as compared to the general membrane, two complementary methods of analysis of CTB gold density were used on influenza virus-infected MDCK and CV1 cells at 6 h p.i. to determine whether GM1 was concentrated in the vicinity of HA (Figs. 3A and D). First, the distance from each 15-nm gold particle to the nearest 6-nm gold particle was measured along the membrane, thus representing the distance separating HA from the nearest CTB staining. These intervals were plotted as histograms for data from both MDCK (Fig. 3B) and CV1 (Fig. 3E) cells. The average density of CTB gold was 0.02 particles/20 nm (or 1 particle per 1000 nm), and since HA staining could be anywhere between CTB particles, the average distance of HA from CTB, if GM1 was randomly distributed, would be 500 nm. The data showed that ~85% of the GM1 staining for both MDCK cells and CV1 cells were less than 500 nm from the nearest 15-nm gold particle. To confirm the co-localization of GM1 and HA, the data were analyzed by a second method. The density of all CTB gold staining was measured along 1 μm of plasma membrane either side of a 15-nm gold particle (Brown and Lyles, 2003a; 2005). If GM1 is preferentially found near HA, CTB gold staining will be most dense at small distances from 15-nm gold particles, while at greater distances from HA, GM1 will be found at the average membrane concentration. The density of GM1 staining surrounding HA in both MDCK (Fig. 3C) and CV1 (Fig. 3F) cells showed an increase inversely proportional to the distance of separation, represented by a region of negative slope. Thus, GM1 was associated with the morphologically identifiable clusters of HA.

NA but not the M2 ion channel protein co-localizes to HA-containing clusters

It has been shown previously that influenza virus NA glycoprotein is associated with lipid rafts using the criteria that NA is insoluble after 1% Triton X-100 extraction at 4 °C (Barman et al., 2004; Barman and Nayak, 2000). To test the specificity and reactivity of an NA polyclonal anti-sera HeLa cells were transfected to express either NA or HA (Figs. 4A and B, respectively). Following fixation, cells were reacted with the anti-NA sera and then an Alexafluor 488-conjugated secondary antibody. Only cells expressing NA exhibited fluorescent staining. HA expression was confirmed by reaction with HA-specific sera (results not shown). To examine the distribution of NA on the surface of infected cells, analytical immunogold electron microscopy was used. Influenza virus-infected MDCK cells at 6 h p.i. were stained simultaneously with rabbit anti-NA and goat anti-HA anti-sera, and antibody binding was detected using donkey anti-rabbit and donkey anti-goat antibodies conjugated to either 15-nm or 6-nm gold particles, respectively (Fig. 4C). The relative amounts of NA present in microdomains are lower than that of HA, and this is consistent with the lower amount of NA than HA found in purified influenza virus (Lamb and Krug, 2001). The majority of the NA staining on the cell surface was found in clusters that also contained HA. NA staining in non-budding regions on random cell profiles was analyzed, and NA was found organized into microdomains of a single size with an average diameter of ~250–400 nm which is in agreement with that found for HA (Fig. 4D). The size estimate for NA-containing microdomains was slightly smaller than that derived from measuring HA most likely because of the relatively lower level of NA staining and the densely packed nature of the HA distribution.

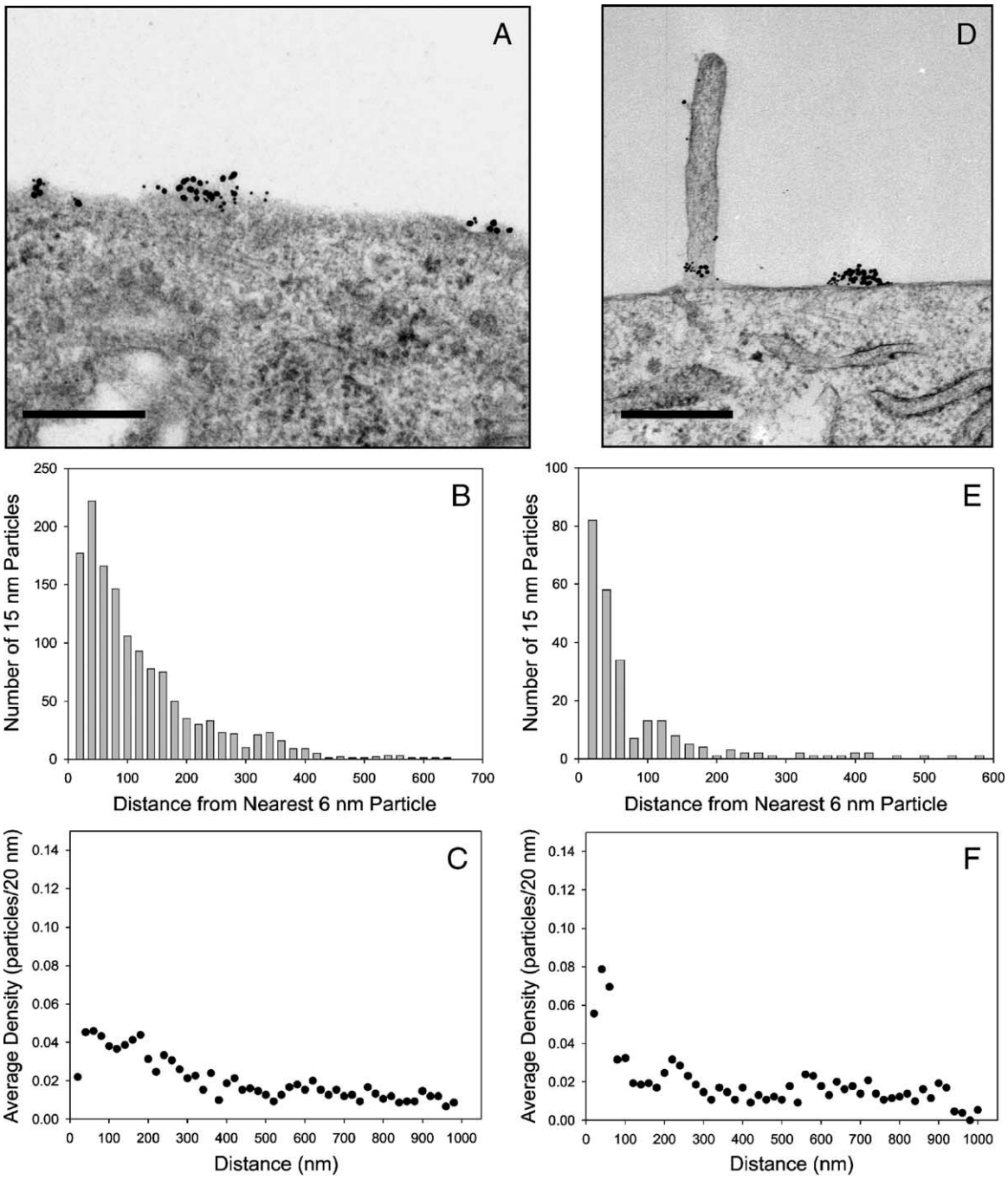

Fig. 3. Influenza virus HA and GM1 are enriched in the same microdomains. The co-localization of GM1 and HA to the same cell surface clusters was investigated in both influenza virus-infected MDCK (A–C) and CV1 (D–F) cells. Influenza virus-infected MDCK (A) or CV1 (D) cells 6 h p.i. were stained with CTB 6-nm gold and goat anti-HA anti-serum followed by donkey anti-goat secondary antibody coupled to 15-nm gold particles. Cells were fixed, embedded and processed for electron microscopy (Scale bar = 0.5 μm). The distance between HA represented by a 15-nm gold particle and the closest CTB 6-nm gold particle was plotted as a histogram of intervals for MDCK (B) and CV1 (E) cells. As a complementary method of analyzing co-localization, the density of CTB staining 1 μm either side of HA was measured and plotted as average density (Brown and Lyles, 2003b; 2005).

The density of HA within the vicinity of NA staining was analyzed to confirm that NA and HA are co-localized in microdomains. Measurement of the distance between NA and the nearest HA staining (Fig. 4E) showed that 95% of NA was found within ~125 nm of HA, this distance is less than or equal to one half the diameter of NA-containing microdomains. Measuring the density of HA 1 μm either side of NA staining (Fig. 4F) showed an increased density of HA in close proximity to NA. These data show that clusters which are enriched in HA do not exclude NA, and the data suggest that both HA and NA proteins are concentrated in these microdomains.

The influenza virus M2 ion channel protein is not associated with lipid rafts (Zhang et al., 2000), even though it is reported to contain a putative cholesterol binding site (Schroeder et al., 2005). Thus, M2 would not be predicted to be found in HA/NA-containing microdomains. However, M2 must be found at

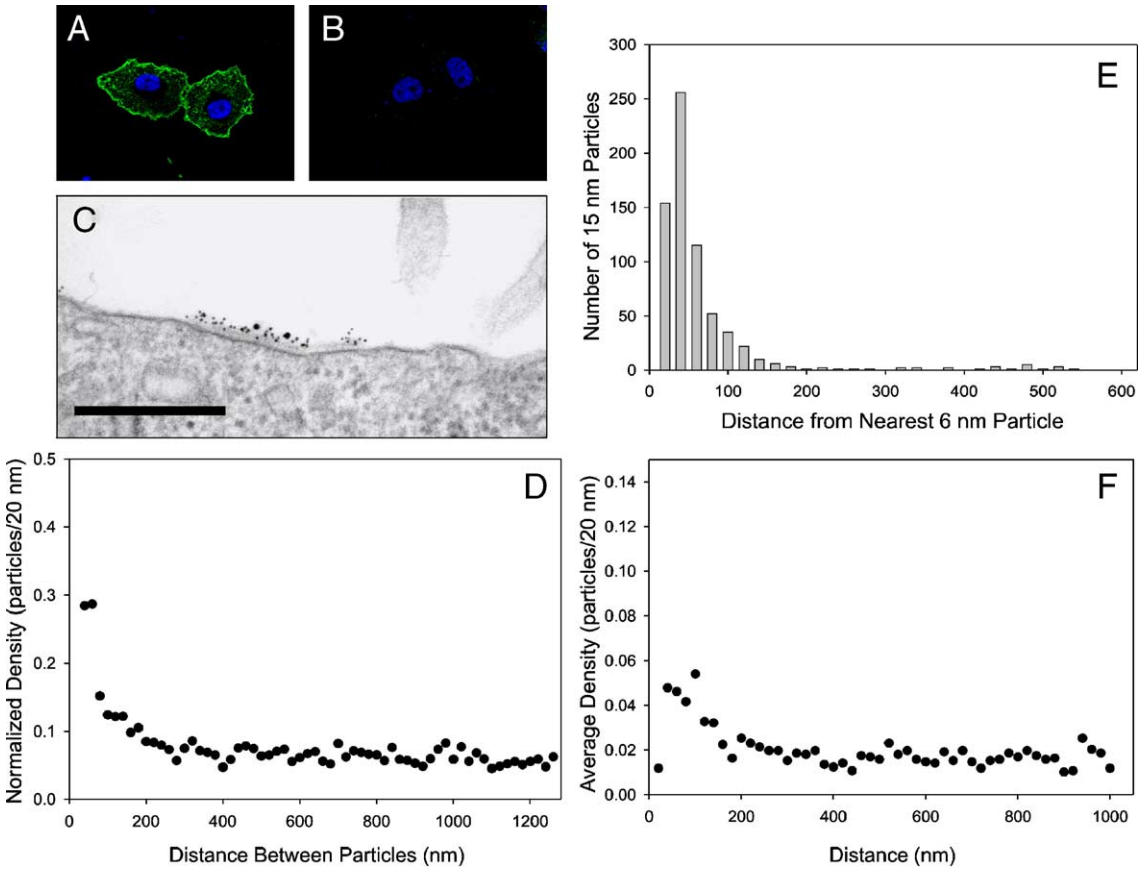

Fig. 4. NA is localized within the same microdomains as HA. To demonstrate the specificity of the anti-NA sera, HeLa cells were grown on glass coverslips and transfected to express either (A) influenza virus NA or (B) influenza virus HA. After fixation, cells were reacted with rabbit anti-serum specific for NA followed by goat anti-rabbit secondary antibodies conjugated to Alexafluor 488. Cells were stained with DAPI, mounted on slides and examined with a Zeiss Axiovert 200 M equipped with an Apotome optical sectioning device. (C) Influenza virus-infected MDCK cells 6 h p.i. were stained with rabbit anti-NA and goat anti-HA-specific sera. Bound immunoglobulins were visualized with donkey anti-rabbit IgG conjugated to 15-nm gold (NA) and donkey anti-goat IgG coupled to 6-nm gold particles (HA). Cells were fixed, embedded and processed for electron microscopy (scale bar = 0.5 μm). (D) The distribution and average density of NA staining were determined by measuring the pair-wise intervals between 15-nm gold particles along the plasma membrane of 38 randomly selected cell profiles. (E) Co-localization of NA and HA within the same membrane microdomains was determined by measuring the distance from each 15-nm gold particle and the nearest 6-nm gold marker along the plasma membrane. (F) The average density of HA staining 1 μm either side of each 15-nm gold particle representing NA.

sites of virus budding as it has to be incorporated into the envelope of progeny virions (Zebedee and Lamb, 1988). To examine the distribution of M2 relative to HA, influenza virus-infected MDCK cells at 6 h p.i. were stained with both goat anti-HA and mouse MAb 14C2 specific for M2. Antibody binding was detected using donkey anti-goat coupled to 15-nm gold and donkey anti-mouse IgG conjugated to 6-nm gold, respectively. HA-containing clusters generally were devoid of M2 staining, whereas M2 staining was visible elsewhere on the plasma membrane (Figs. 5A and B, arrows). As a small number of M2 molecules are incorporated into progeny virions, some M2 staining would be expected to be present at sites of virus assembly, and as shown in Fig. 5C (arrow), a budding influenza virus attached to the cell membrane does exhibit M2 staining. The low density of M2 staining did not allow for an assessment of its surface distribution or a meaningful nearest neighbor analysis. However, it was possible to evaluate the density of HA staining surrounding M2 in non-budding membrane regions (Fig. 5D). The average densities of HA within 1 μm of M2 is best described by a straight line of 0 slope, indicating no change in the concentration of HA relative to the location of the M2 protein, indicating HA and M2 show little association outside the budozone.

The data shown above indicate that in influenza virus-infected cells, HA and NA segregate into ~425- to 600-nm microdomains that contain the lipid raft maker GM1. To determine whether the lipid microdomain association is an intrinsic property of HA or driven by an association of the HA with the viral matrix protein, we examined HA distribution in an MDCK cell line stably expressing HA (MDCK-HA). HA (15-nm gold particles) was visible in clusters similar in appearance to those seen in virus-infected cells (Fig. 6A). Analysis of the gold particle distribution in these micrographs showed that the size of the HA-containing microdomains was ~350–550 nm in diameter which is close to the ~325- to 500-nm diameter microdomain observed for MDCK cells 4 h p.i. Thus, the average membrane density in MDCK-HA cells is very similar to the distribution of HA in virus-infected cells at 4 h p.i., suggesting that the association of HA into these microdomains is an intrinsic property of the HA protein, but that the relative size of the microdomain may be a function of the HA expression level. Recently, Hess et al. (2005) found for

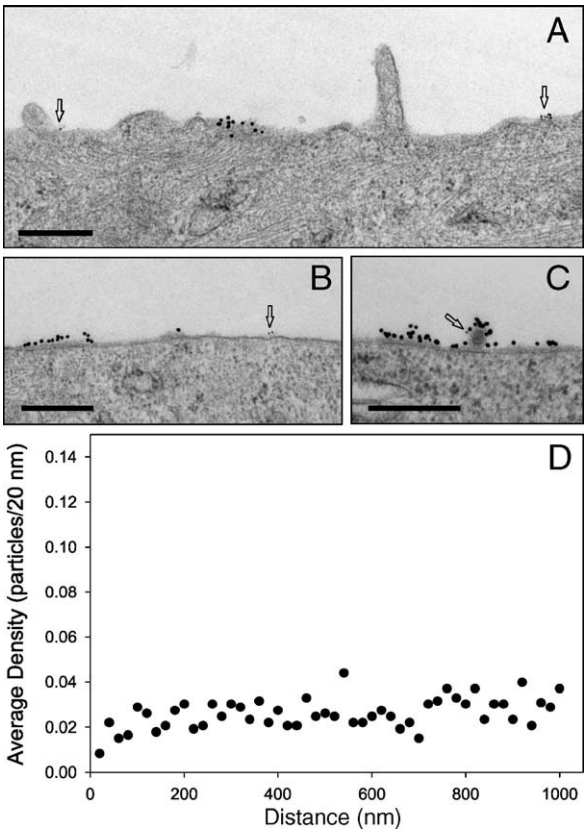

Fig. 5. The influenza virus M2 protein-selective ion channel protein is not associated with HA-containing microdomains. (A–C) Influenza virus-infected MDCK cells 6 h p.i. were stained with M2-specific mouse MAb 14C2 and goat anti-HA sera. The binding of M2- or HA-specific immunoglobulins was detected by host-specific secondary antibodies conjugated to 6-nm and 15-nm gold particles, respectively. Cells were fixed, embedded and processed for electron microscopy. Arrows denote sites of M2 staining (scale bar = 0.5 μm). (D) The density of HA within 1 μm either side of M2 staining was measured to detect possible co-localization of both markers in the same microdomain. The data were derived from 26 micrographs.

a stably transfected cell line expressing the H2 subtype HA that there was a non-random distribution of HA with a bias towards a cluster size in the range of 500–900 nm.

Clusters of HA/GM1 grow in size with time

The analysis of HA and GM1 organization in the plasma membrane was confined necessarily to the 60–80 nm depth of a thin section. To expand the depth of the region analyzed, infected cells were immunogold stained for GM1 and HA as above and sectioned serially so that the same cell, randomly selected, could be examined across the expanse of several continuous sections. The tracings of the plasma membrane profiles were arranged in sequential order with the location of HA represented by closed blue circles and GM1 staining by red. In Fig. 7A, the cell surface topography of a virus-infected MDCK cell at 4 h p.i. is shown. Clusters of HA at this point rarely extended across more than 3–4 sections, and most HA microdomains were associated with GM1 either laterally or axially. This is observed more readily when the labeling data from Fig. 7A is arranged as if viewed from above the cell (Fig. 7B). A similar analysis of several sections obtained from virus-infected MDCK cells at 6 h p.i. (Figs. 7C and D) reinforces the conclusion that HA clusters are associated with GM1. Frequently, CTB gold staining was located at the periphery of HA clusters, thus confirming the earlier observations made on single thin sections that CTB gold was more frequently encountered on the edge of microdomains and in areas where HA was apparently less dense, although the possibility that the lipid composition of the HA clusters changes over time cannot be ruled out. At 4 h p.i., it was difficult to identify positively all HA microdomains due to the lower expression level; however, roughly the same number of HA clusters were evident at 4 h p.i. as at 6 h p.i. per unit length of membrane. By 6 h p.i., HA clusters had grown in size and density and were visualized on the surface of the cell, frequently extending across 5–7 sections (Fig. 7D). When areas of virus assembly were encountered, the size and density of HA clusters increased to a greater extent. Examination of two regions of virus budding from virus-infected MDCK cells at 6 h p.i. (Figs. 7E and F, delineated by red boxes) showed that the area and degree of HA concentration was much greater than observed for non-budding regions of membrane.

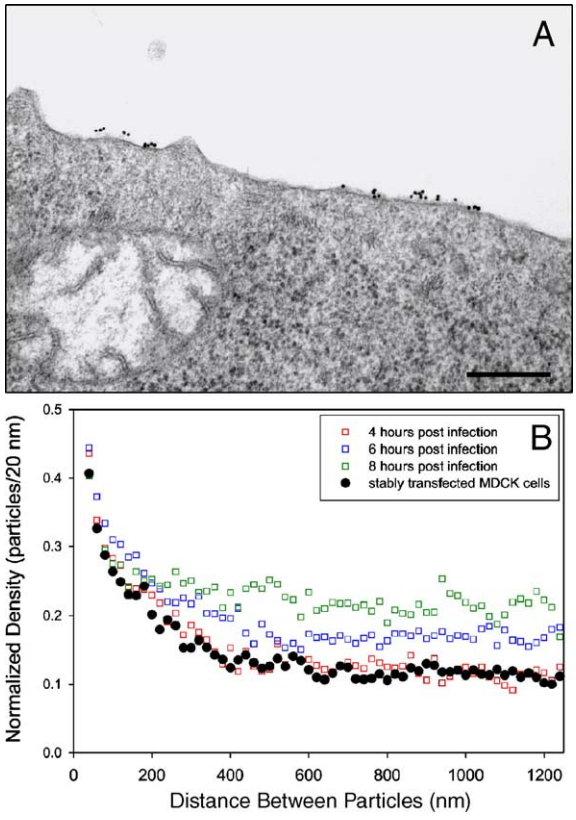

Fig. 6. Clustering of HA in microdomains is due to an intrinsic property of the HA protein. (A) MDCK-HA cells stably transfected to express HA were reacted with goat anti-HA sera followed by donkey anti-goat antibodies conjugated to 15-nm gold particles. Following fixation, cells were infiltrated and processed for electron microscopy. (B) The average cell surface density and distribution of HA were determined from 28 randomly acquired cell profiles. These results were compared to the data obtained from MDCK cells 4, 6 and 8 h p.i. as shown in Fig. 1C.

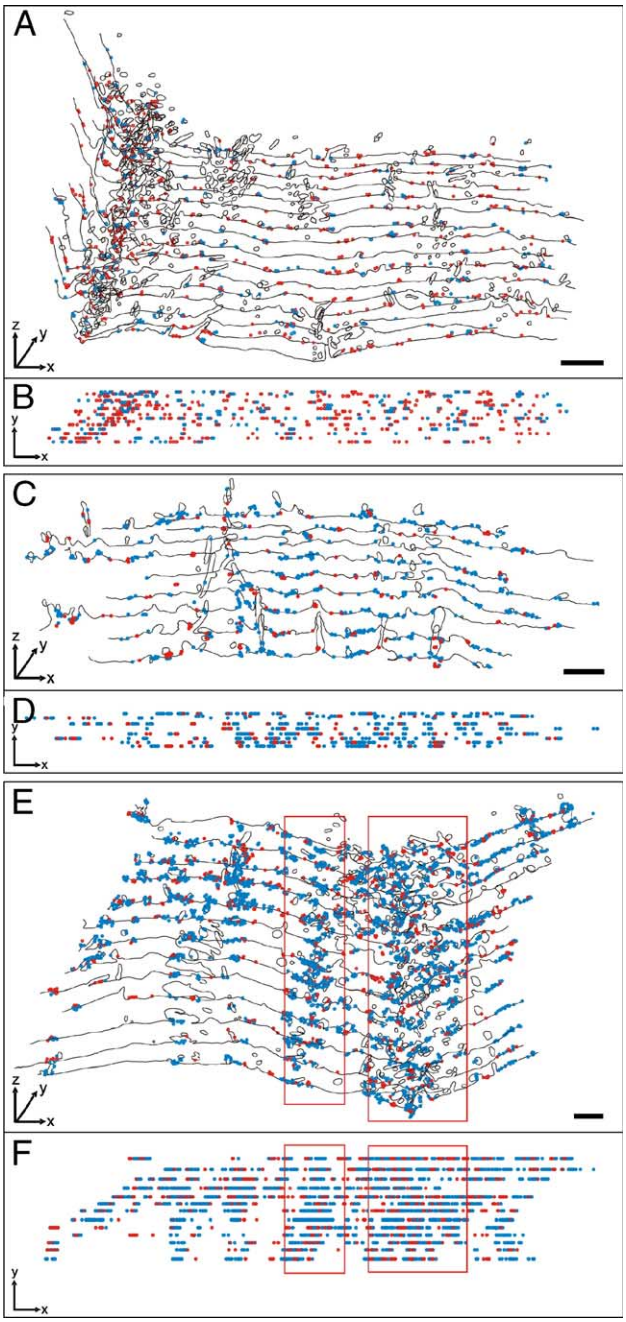

Fig. 7. HA/GM1-containing microdomains increase in size with time p.i. Influenza virus-infected MDCK cells were harvested at 4 (A, B) or 6 (C–F) h p.i. Cells were stained to visualize HA and GM1 as described above. Samples were processed for electron microscopy, and ribbons of sections of consistent thickness were transferred to slot grids. The same cell was identified in each section of the ribbon, and the same region of the cell was photographed. Plasma membranes were traced, and the location of HA was shown using blue circles, and GM1 was represented by red circles. Membrane tracings were arranged from the perspective of cell surface topography (A, C, E), or the staining was arranged solely in the x, y dimensions as if viewed from above with no contribution from cell surface elevation (B, D, F). (A, B) MDCK cells 4 h p.i. showing non-budding regions of cell plasma membrane. The tracing shown is a representative example of 17 sets of serial sections for this time point ranging in depth from 10 to 17 sections. (C, D) The tracings are derived from MDCK cells 6 h p.i. showing non-budding region of the cell surface. (E, F) MDCK cells 6 h p.i. showing regions of viral budding activity delineated by red boxes. Panels C–F are representative of serial sections taken at 6 h p.i. and selected from 11 data sets comprised of between 9 to 13 sections each (scale bar = 1.0 μm).

HA microdomains on the surface of infected cells are disrupted by depletion of cellular cholesterol, and the integrity of lipid rafts can be disrupted by the removal of cellular cholesterol (Keller and Simons, 1998). To test the effect of cholesterol depletion on the clustering of HA, MDCK cells were grown in the presence of 10 μM mevastatin and 250 μM mevalonic acid lactone for 48 h. The cells were then infected with influenza virus, and at 3 h p.i., the culture media were replaced with media containing 10 mM methyl-β-cyclodextrin and incubated for 1 h. This treatment reduced the cellular cholesterol level by an average of 63.9% (n = 2), when compared to uninfected control cells. The treated MDCK cells at 4 h p.i. were immunogold stained for HA and prepared for electron microscopy. The HA labeling on the surface of cholesterol-depleted cells was analyzed for microdomain organization and compared to untreated, infected cells labeled in parallel. As the morphology of the cholesterol-depleted cells was variable, the sample size of the data set was increased to 57 cell profiles encompassing 3523 gold particles over ~340-μm cell membrane. An example of the morphology and labeling pattern of a cholesterol-depleted cell is shown in Fig. 8A. The analysis of HA microdomains showed that the diameter

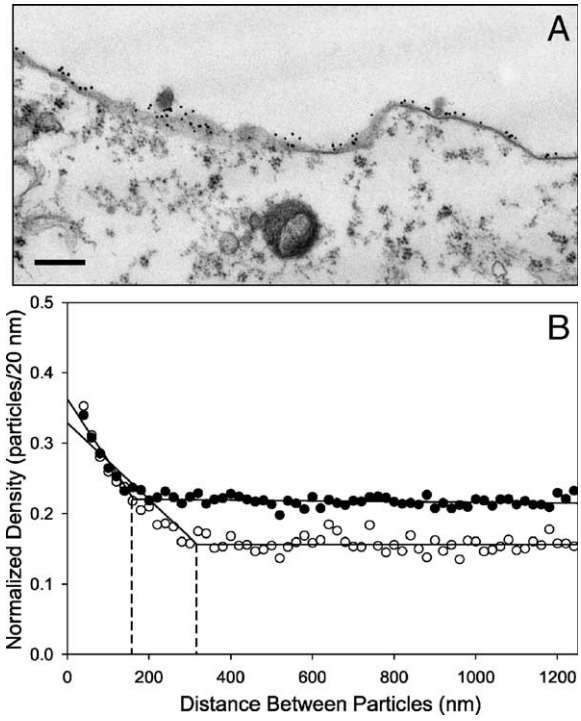

Fig. 8. The structural integrity of HA-containing microdomains is dependent upon the presence of cholesterol. MDCK cells were incubated for 48 h in the presence of 10 μM mevastatin and 250 μM mevalonic acid lactone. The cells were then infected with influenza virus and at 3 h p.i. were extracted for 1 h in the presence of 10 mM methyl-β-cyclodextrin. The infected cells (4 h p.i.) were labeled for HA and processed for electron microscopy as described above. (A) Image of cholesterol-depleted MDCK cells showing HA staining on the cell surface. (B) The average density and distribution of HA on the surface of cholesterol-depleted cells (●) was compared to control infected MDCK cells (○) stained in parallel. Due to the variability in morphology of the cholesterol-depleted cells, 57 cell profiles encompassing 3523 gold particles were used to generate the cholesterol depletion data. For the control sample, the analysis was carried out on 1439 gold particles over 34 cell profiles.

decreased from ~325–500 nm in the control to approximately ~150–250 nm in cholesterol-depleted cells (Fig. 8B). There was an apparent increase in the average membrane concentration of HA from 0.155 to 0.22 particles/20 nm. Presumably, the disruption of densely packed microdomains caused the dispersal of HA in the plasma membrane where it was more accessible to binding by antibodies, although our data do not rule out the possibility that cholesterol depletion increases the level of surface HA. Hess et al. (2005) also found that HA clusters were disrupted, but not abolished, when the lipid composition of membranes of an HA-expressing cell line was altered. Thus, the distribution of HA on the surface of cholesterol-depleted cells provides further evidence that HA-containing microdomains are raft-like membranes.

Discussion

It is now well established that HA and NA of influenza virus associate intrinsically with lipid raft microdomains (Barman and Nayak, 2000; Fiedler et al., 1993; Kundu et al., 1996; Lin et al., 1998; Melkonian et al., 1999; Scheiffele et al., 1999; Scheiffele et al., 1997; Simons and Ikonen, 1997; Takeda et al., 2003; Zhang et al., 2000). Residues in the transmembrane domains of HA and NA are important for raft association (Barman and Nayak, 2000; Lin et al., 1998; Takeda et al., 2003), and deletion of the cytoplasmic tail of HA and NA can affect raft association. The lipid composition of purified influenza virus reflects that of lipid rafts (Scheiffele et al., 1999; Zhang et al., 2000), suggesting that influenza virus buds from raft-like microdomains. It has also been suggested that the similarity in lipid composition between rafts and some enveloped viruses may be serendipitous because 40–70% of the plasma membrane is comprised of lipid rafts (Fridriksson et al., 1999; Mayor and Maxfield, 1995). However, this seems unlikely for influenza virus as wild-type HA is observed by immunogold electron microscopy to associate with discrete patches of plasma membrane, whereas HA-containing mutations in the transmembrane domain that ablate raft association cause HA to be randomly distributed over the plasma membrane (Takeda et al., 2003).

To examine the distribution of influenza virus HA, NA and M2 proteins at the plasma membrane of infected cells at different times after infection, we used analytical immunogold electron microscopy, quantifying the data using the approaches of Ripley (1979), Philimonenko et al. (2000) and Brown and Lyles (2003a, 2003b, 2005). HA was found in clusters that grew in size with time from ~325 to ~600 nm. The data suggest these patches become the sites of viral budding termed the viral budozone (Schmitt and Lamb, 2004). NA was also found in clusters of very similar size, and HA and NA were found in the same population of membrane microdomains. The ganglioside GM1, a marker for detergent-resistant membranes, showed a co-localization surrounding the HA clusters, providing evidence from a microscopy approach that the HA and NA are in sphingomyelin/cholesterol-enriched lipid microdomains. Depletion of cholesterol from cells decreased the diameter of the HA clusters by ~175–250 nm, consistent with the HA-containing microdomains being raft-like microdomains that are disrupted on depletion of cholesterol. In contrast, and confirming biochemical evidence obtained previously (Zhang et al., 2000), the M2 ion channel protein is localized at the plasma membrane independently of HA and NA proteins.

Analysis of the size of the HA-containing lipid microdomains in MDCK cells indicated that at 4 h p.i., the microdomains were ~325–500 nm in diameter, and by 6 h p.i., they grew to ~425–600 nm in diameter. These diameters are much larger than those commonly associated with rafts, and the HA- and NA-containing microdomains may represent amalgamations of individual rafts. In influenza virus-infected CV1 cells, the clusters of HA had a smaller diameter than compared to MDCK cells and showed less HA-staining suggesting a lower membrane concentration. These observations support the idea that the size of the HA clusters in non-budding regions of the plasma membrane is dependent upon the expression levels of HA and is dependent on cell type. Related observations leading to similar conclusions have been made with HIV gag (Lindwasser and Resh, 2001), the Src family kinase, Fyn (Webb et al., 2000) and the non-raft associated VSV G protein (Brown and Lyles, 2003a).

Examination of stacks of serial sections of influenza virus-infected MDCK cells, at 4 h and 6 h p.i., provided a high-resolution reconstruction of the arrangement of HA and GM1 across the cell surface, eliminating the constraint of studying a single 60- to 80-nm-thick thin section. The data indicate that the number of sites of HA clusters does not change greatly from 4 h to 6 h p.i., but the average diameter of the clusters increases later in infection. As HA expressed in a stably transfected cell line also forms clusters, it indicates that the ability to form these large raft-like clusters is an intrinsic property of HA. In HIV-infected cells multimerization of Gag regulates its association with clustered rafts, forming so-called “barges” of rafts (Lindwasser and Resh, 2001).

When an area of virus budding was encountered in the serial section data set, the cluster of immunogold-labeled HA has a greater diameter (ranging from 2 to 5.5 μm) than individual HA microdomains in non-budding regions at the same time p.i. (Figs. 7E and F). These viral budozone assembly sites are distinguished from HA-containing microdomains by the presence of other viral proteins including the non-raft associated M2 protein. It is not known what triggers the formation of these assembly sites, but the influenza virus matrix (M1) protein is often considered as the catalyst for nucleation of viral components. Interactions of the cytoplasmic tails of the HA and NA with M1 may drive the assembly of HA- and NA-containing clusters into the viral assembly site by cross-linking individual microdomains. Analysis of the assembly of influenza viruses containing truncations to both the HA and NA cytoplasmic tails has shown the importance of these cytoplasmic tails in assembly (Jin et al., 1997). Furthermore, the budding site must permit inclusion of regions of membrane containing non-raft associated M2 protein, a process that may be stochastic or alternatively driven by association of M1 protein assembled on the cytoplasmic face of the membrane. Evidence for a determinant in the ectodomain of M2 that is

necessary for its inclusion into nascent virions supports the idea that the levels of M2 in viruses are the result of specific interactions (Park et al., 1998). Furthermore, the amount of M2 incorporated into virions is not significantly dependent upon cellular expression levels (Bourmakina and Garcia-Sastre, 2005). Recently, it has been suggested that the cytoplasmic tail of M2 protein plays a role in virus formation via interacting with the viral ribonucleoprotein complexes (McCown and Pekosz, 2005). It cannot be ruled out that either a small amount of M2 sufficient for inclusion into virions finds its way into raft clusters, or that M2 inclusion into nascent virions is driven by an association with other viral proteins which occurs at a time p.i. not examined in this study. Vesicular stomatitis virus (VSV) pseudotypes containing HA are readily obtainable, and these particles are presumably formed by incorporating raft-associated HA and non-raft associated VSV G protein. Also, Brown and Lyles (2005) have shown that a recombinant VSV that expresses CD4 incorporates into its envelope both VSV G protein and CD4, yet VSV G and CD4 reside in separate non-raft lipid microdomains. Thus, unless the segregation to microdomains is dynamic and in constant flux, the enveloped virus assembly machinery must allow the inclusion of non-raft-associated and raft-associated proteins into the nascent viral particle.

Materials and methods

Cells, viruses, plasmids, immune reagents and chemicals

Madin–Darby canine kidney (MDCK) cells, CV1 cells and HeLa-T4 cells were maintained as previously described (Paterson and Lamb, 1993). The MDCK cell line stably expressing influenza hemagglutinin (HA) (A/Udorn/72) has been described previously (Takeda et al., 2003). Influenza stocks were prepared and infections performed at a multiplicity of infection of 5 as described (Paterson and Lamb, 1993). The expression plasmid pCAGGS was used to express the cDNAs of HA or NA of influenza virus (A/Udorn/72). Rabbit anti-serum specific for NA was generously provided by Gillian Air. Goat antibodies specific for A/Udorn/72 HA have been described (Zhang et al., 2000). The 14C2 M2-specific MAb has been described previously (Zebedee and Lamb, 1988). Host specific, unconjugated, affinity purified immunoglobulins for the production of gold-coupled secondary antibodies were obtained from Jackson Immunoresearch Laboratories, Inc. (West Grove, PA). Cholera toxin, subunit B (CTB) was obtained from Calbiochem (La Jolla, CA). Other chemicals were from Sigma (St. Louis, MO) unless otherwise noted.

Electron microscopy and quantification of gold staining

Colloidal gold and antibody-gold conjugates were prepared as described (Slot and Geuze, 1985). Cholera toxin B (CTB) gold conjugates were made according to Parton (1994). The HA-specific goat serum was used at a 1:200 dilution, the NA-specific rabbit serum at 1:300 dilution and the M2-specific mouse MAb was used at 1:300 dilution. MDCK cells at varying times post-infection (p.i.) were incubated with incubation buffer (0.1 M phosphate buffer, pH7.1 containing 0.1% bovine serum albumin and 1% cold water fish gelatin (Electron Microscopy Sciences, Fort Washington, PA) for 30 min. This and all subsequent steps were carried out at 4 °C. Cells were reacted with CTB gold conjugate, diluted in incubation buffer to an approximate protein concentration of 10 μg/ml, for 60 min with gentle rocking. After washing with 3 changes of incubation buffer over 30 min, the cells were incubated with goat anti-HA antibody diluted in incubation buffer. Samples were washed with 6 changes of incubation buffer over 60 min and incubated with gold-coupled secondary antibodies for 1 h with gentle rocking. Finally, cells were washed with 3 changes incubation buffer over 30 min followed by 3 changes of 0.1 M phosphate buffer, pH 7.1 (PB). Samples were fixed in 2% glutaraldehyde in PB overnight at 4 °C. After washing in 6 changes PB over 60 min at room temperature, cells were post-fixed in 1% osmium tetroxide in PB for 1 h. Following washing as above, cells were dehydrated in a graded ethanol series, released from culture dishes by treatment with propylene oxide and then infiltrated and embedded in epoxy resin according to standard protocols.

Thin sections were collected on parllodion-coated 200 mesh copper grids, or in the case of serial sections, similarly coated 1 × 0.5 mm copper slot grids. Samples were stained with uranyl acetate and lead citrate according to standard procedures and examined with either a Jeol JEM-100CX II or Jeol 1230, operating at 80 kV. The sections used for this study exhibited silver and occasionally light gold interference colors and therefore predominantly ranged in thickness from 60 to 80 nm (Peachey, 1958). Micrographs were taken at either ×36,000 or ×30,000, except for serial sections, and these were photographed at ×10,000. The plasma membrane profiles of cells photographed in serial sections were made and arranged using CorelDraw Graphics Suite 12 (Ottawa, Ontario, Canada).

The quantification of gold staining was performed based on the methods developed by Ripley (1979), Philimonenko et al. (2000) and Brown and Lyles (2003a). Briefly, approximately 25 micrographs of randomly selected cells that did not include regions of virus budding were acquired for each sample. Each micrograph was obtained from a different cell, except for serial sections. For each image, the intervals between the left most gold particle and each gold particle to the right were measured using Image J (NIH, Bethesda, MD). These values were transferred to a spreadsheet where the pair-wise measurement was calculated along the plasma membrane between each gold particle and every other gold particle to its right. This yielded a set of data that provided the distances between every plasma membrane associated gold particle on a micrograph. These sets of intervals were plotted as histograms of the average number of gold particles (y-axis) separated by a given distance (20 nm) along the plasma membrane (x-axis). The values along the y-axis were normalized and expressed as the average number of gold particles per 20-nm interval. The average general density, i.e., both microdomain and inter-domain labeling, was provid-

ed by extending the portion of the plot having a slope of 0 to intercept the *y*-axis. A break in this line leading to a negative change in slope indicated that the labeled protein was organized into a membrane microdomain. Drawing a perpendicular line from the point of slope change to intercept the *x*-axis provided the value for on the average 64% of the diameter for a given population of microdomains (Brown and Lyles, 2003a). Two changes in slope were indicative of two populations of microdomains of different size. Three or more changes in slope were difficult to identify and were described by a curved line. The criteria of Brown and Lyles (2003a) were adopted for determining slope changes in the plotted data. The data were corrected for distance from the right edge of the micrograph as described (Brown and Lyles, 2003a). Least squares analysis of the data was performed using Minitab 12 (Minitab, Inc., State College, PA). Occasionally, the data for the interval of 0–20 nm would be lower than expected, this was likely caused by the physical size of the antibodies and the gold particles (Philimonenko et al., 2000).

The co-localization of two different membrane proteins was determined by two complementary methods. First, Image J was used to measure the distance between one protein and the nearest second protein of interest, a so-called nearest neighbor analysis. These data were plotted as a histogram of the average density of gold particles plotted per 20 nm increment of distance separating the two markers. The second approach involved using Image J to measure the density of gold particles staining one protein of interest 1 μm either side of the second protein (Brown and Lyles, 2003b, 2005). If two proteins localize to the same structure or membrane region, the density of the first protein will be higher on average as the distance from the second protein decreases. Clusters of HA were counted on serial section sets by using the $x-y$ data to find groupings of HA staining. At 4 h p.i., small clusters of HA could not always be identified, and at 6 h p.i., the boundaries between clusters were obscured in both cases due to HA expression levels. To counter these potential problems, 5 or more sets of serial sections, of at least 10 sections each, were analyzed for each time point.

Indirect immunofluorescence

The specificity of NA-specific rabbit anti-serum was tested by staining the surface of HeLa cells that were transfected to express influenza virus HA or NA. Immunofluorescence was performed as described (Leser et al., 1996) except that host-specific secondary antibodies conjugated to Alexafluor 488 (Molecular Probes, Eugene, OR) were used, and cells were stained with DAPI according to standard protocols. Cells were examined with a Zeiss Axiovert 200M equipped with an Apotome optical sectioning device.

Cholesterol depletion

Cells were grown for 48 h in complete media containing 10 μM mevastatin and 250 μM mevalonic acid lactone (Carrasco et al., 2004). Cultures were infected with virus influenza, and 3 hr p.i., the media were replaced with media containing 10 mM methyl-β-cyclodextrin (Keller and Simons, 1998). After 1-h incubation (4 h p.i.), cells were labeled and processed for electron microscopy as described above. Cholesterol levels in lysates prepared from parallel cell cultures were assayed in triplicate for cholesterol content using the Amplex Red cholesterol assay (Molecular Probes, Eugene, OR).

Acknowledgments

We thank Dr. Douglas Lyles (Wake Forest University Medical School) for helpful discussions and Christopher Ratcliff for helping to digitalize hundreds of thousands of gold particles. The Jeol 1230 electron microscope used in this study is part of the Biological Imaging Facility at Northwestern University, Evanston, IL. We are grateful to the Howard Hughes Medical Institute for major funding towards the purchase of the Jeol 1230 microscope. This work was supported in part by research grants R37 AI-20201 and R01 AI-23173 from the National Institute of Allergy and Infectious Diseases. RAL is an investigator of the Howard Hughes Medical Institute.

References

Ahmed, S.N., Brown, D.A., London, E., 1997. On the origin of sphingolipid/cholesterol-rich detergent-insoluble cell membranes: physiological concentrations of cholesterol and sphingolipid induce formation of a detergent-insoluble, liquid-ordered lipid phase in model membranes. Biochemistry 36, 10944–10953.

Barman, S., Nayak, D.P., 2000. Analysis of the transmembrane domain of influenza virus neuraminidase, a type II transmembrane glycoprotein, for apical sorting and raft association. J. Virol. 74, 6538–6545.

Barman, S., Adhikary, L., Chakrabarti, A.K., Bernas, C., Kawaoka, Y., Nayak, D.P., 2004. Role of transmembrane domain and cytoplasmic tail amino acid sequences of influenza a virus neuraminidase in raft association and virus budding. J. Virol. 78, 5258–5269.

Bavari, S., Bosio, C.M., Wiegand, E., Ruthel, G., Will, A.B., Geisbert, T.W., Hevey, M., Schmaljohn, C., Schmaljohn, A., Aman, M.J., 2002. Lipid raft microdomains: a gateway for compartmentalized trafficking of Ebola and Marburg viruses. J. Exp. Med. 195, 593–602.

Bourmakina, S.V., Garcia-Sastre, A., 2005. The morphology and composition of influenza A virus particles are not affected by low levels of M1 and M2 proteins in infected cells. J. Virol. 79, 7926–7932.

Brown, D.A., Rose, J.K., 1992. Sorting of GPI-anchored proteins to glycolipid-enriched membrane subdomains during transport to the apical cell surface. Cell 68, 533–544.

Brown, E.L., Lyles, D.S., 2003a. A novel method for analysis of membrane microdomains: vesicular stomatitis virus glycoprotein microdomains change in size during infection, and those outside of budding sites resemble sites of virus budding. Virology 310, 343–358.

Brown, E.L., Lyles, D.S., 2003b. Organization of the vesicular stomatitis virus glycoprotein into membrane microdomains occurs independently of intracellular viral components. J. Virol. 77, 3985–3992.

Brown, E.L., Lyles, D.S., 2005. Pseudotypes of vesicular stomatitis virus with CD4 formed by clustering of membrane microdomains during budding. J. Virol. 79, 7077–7086.

Carrasco, M., Amorim, M.J., Digard, P., 2004. Lipid raft-dependent targeting of the influenza A virus nucleoprotein to the apical plasma membrane. Traffic 5, 979–992.

Chamberlain, L.H., 2004. Detergents as tools for the purification and classification of lipid rafts. FEBS Lett. 559, 1–5.

Compans, R.W., Dimmock, N.J., 1969. An electron microscopic study of single-cycle infection of chick embryo fibroblasts by influenza virus. Virology 39, 499–515.

Fiedler, K., Kobayashi, T., Kurzchalia, T.V., Simons, K., 1993. Glycosphingolipid-enriched, detergent-insoluble complexes in protein sorting in epithelial cells. Biochemistry 32, 6365–6373.

Fridriksson, E.K., Shipkova, P.A., Sheets, E.D., Holowka, D., Baird, B., McLafferty, F.W., 1999. Quantitative analysis of phospholipids in functionally important membrane domains from RBL-2H3 mast cells using tandem high-resolution mass spectrometry. Biochemistry 38, 8056–8063.

Glebov, O.O., Nichols, B.J., 2004. Lipid raft proteins have a random distribution during localized activation of the T-cell receptor. Nat. Cell Biol. 6, 238–243.

Gomez-Mouton, C., Abad, J.L., Mira, E., Lacalle, R.A., Gallardo, E., Jimenez-Baranda, S., Illa, I., Bernad, A., Manes, S., Martinez, A.C., 2001. Segregation of leading-edge and uropod components into specific lipid rafts during T cell polarization. Proc. Natl. Acad. Sci. U.S.A. 98, 9642–9647.

Hess, S.T., Kumar, M., Verma, A., Farrington, J., Kenworthy, A., Zimmerberg, J., 2005. Quantitative electron microscopy and fluorescence spectroscopy of the membrane distribution of influenza hemagglutinin. J. Cell Biol. 169, 965–976.

Hooper, N.M., 1999. Detergent-insoluble glycosphingolipid/cholesterol-rich membrane domains, lipid rafts and caveolae (review). Mol. Membr. Biol. 16, 145–156.

Jin, H., Leser, G.P., Zhang, J., Lamb, R.A., 1997. Influenza virus hemagglutinin and neuraminidase cytoplasmic tails control particle shape. EMBO J. 16, 1236–1247.

Keller, P., Simons, K., 1998. Cholesterol is required for surface transport of influenza virus hemagglutinin. J. Cell Biol. 140, 1357–1367.

Kenworthy, A.K., Petranova, N., Edidin, M., 2000. High-resolution FRET microscopy of cholera toxin B-subunit and GPI-anchored proteins in cell plasma membranes. Mol. Biol. Cell 11, 1645–1655.

Kundu, A., Avalos, R.T., Sanderson, C.M., Nayak, D.P., 1996. Transmembrane domain of influenza virus neuraminidase, a type II protein, possesses an apical sorting signal in polarized MDCK cells. J. Virol. 70, 6508–6515.

Lamb, R.A., Krug, R.M., 2001. Orthomyxoviridae: the viruses and their replication. In: Knipe, D.M., Howley, P.M. (Eds.), Fields Virology, 4th ed. Lippincott, Williams and Wilkins, Philadelphia, pp. 1487–1531.

Langlet, C., Bernard, A.M., Drevot, P., He, H.T., 2000. Membrane rafts and signaling by the multichain immune recognition receptors. Curr. Opin. Immunol. 12, 250–255.

Laux, T., Fukami, K., Thelen, M., Golub, T., Frey, D., Caroni, P., 2000. GAP43, MARCKS, and CAP23 modulate PI(4,5)P(2) at plasmalemmal rafts, and regulate cell cortex actin dynamics through a common mechanism. J. Cell Biol. 149, 1455–1472.

Leser, G.P., Ector, K.J., Lamb, R.A., 1996. The paramyxovirus simian virus 5 hemagglutinin-neuraminidase glycoprotein, but not the fusion glycoprotein, is internalized via coated pits and enters the endocytic pathway. Mol. Biol. Cell 7, 155–172.

Lin, S., Naim, H.Y., Rodriguez, A.C., Roth, M.G., 1998. Mutations in the middle of the transmembrane domain reverse the polarity of transport of the influenza virus hemagglutinin in MDCK epithelial cells. J. Cell Biol. 142, 51–57.

Lindwasser, O.W., Resh, M.D., 2001. Multimerization of human immunodeficiency virus type 1 Gag promotes its localization to barges, raft-like membrane microdomains. J. Virol. 75, 7913–7924.

Mayor, S., Maxfield, F.R., 1995. Insolubility and redistribution of GPI-anchored proteins at the cell surface after detergent treatment. Mol. Biol. Cell 6, 929–944.

McCown, M.F., Pekosz, A., 2005. The influenza A virus M2 cytoplasmic tail is required for infectious virus production and efficient genome packaging. J. Virol. 79, 3595–3605.

Melkonian, K.A., Ostermeyer, A.G., Chen, J.Z., Roth, M.G., Brown, D.A., 1999. Role of lipid modifications in targeting proteins to detergent-resistant membrane rafts. Many raft proteins are acylated, while few are prenylated. J. Biol. Chem. 274, 3910–3917.

Morgan, C., Hsu, K.C., Rifkind, R.A., Knox, A.W., Rose, H.M., 1961. The application of ferritin-conjugated antibody to electron microscopic studies of influenza virus in infected cells. J. Exp. Med. 114, 825–832.

Munro, S., 2003. Lipid rafts: elusive or illusive? Cell 115, 377–388.

Nguyen, D.H., Hildreth, J.E., 2000. Evidence for budding of human immunodeficiency virus type 1 selectively from glycolipid-enriched membrane lipid rafts. J. Virol. 74, 3264–3272.

Ono, A., Freed, E.O., 2001. Plasma membrane rafts play a critical role in HIV-1 assembly and release. Proc. Natl. Acad. Sci. U.S.A. 98, 13925–13930.

Park, E.K., Castrucci, M.R., Portner, A., Kawaoka, Y., 1998. The M2 ectodomain is important for its incorporation into influenza A virions. J. Virol. 72, 2449–2455.

Parton, R.G., 1994. Ultrastructural localization of gangliosides; GM1 is concentrated in caveolae. J. Histochem. Cytochem. 42, 155–166.

Paterson, R.G., Lamb, R.A., 1993. The molecular biology of influenza viruses and paramyxoviruses. In: Davidson, A., Elliott, R.M. (Eds.), Molecular Virology: A Practical Approach. IRL Oxford Univ. Press, Oxford, pp. 35–73.

Peachey, L.D., 1958. Thin sections I. A study of section thickness and physical distortion produced during microtomy. J. Biophysic. Biochem. Cytol. 4, 233–242.

Philimonenko, A.A., Jnacek, J., Hozak, P., 2000. Statistical evaluation of colocalization patterns in immunogold labeling experiments. J. Struct. Biol. 132, 201–210.

Pralle, A., Keller, P., Florin, E.-L., Simons, K., Horber, J.K.H., 2000. Sphingolipid-cholesterol rafts diffuse as small entities in the plasma membrane of mammalian cells. J. Cell Biol. 148, 997–1007.

Prior, I.A., Harding, A., Yan, J., Sluimer, J., Parton, R.G., Hancock, J.F., 2001. GTP-dependent segregation of H-ras from lipid rafts is required for biological activity. Nat. Cell Biol. 3, 368–375.

Rietveld, A., Simons, K., 1998. The differential miscibility of lipids as the basis for the formation of functional membrane rafts. Biochim. Biophys. Acta 1376, 467–479.

Ripley, B.D., 1979. Test of 'randomness' for spatial point patterns. J. R. Stat. Soc. B41, 368–374.

Robbins, S.M., Quintrell, N.A., Bishop, J.M., 1995. Myristoylation and differential palmitoylation of the HCK protein-tyrosine kinases govern their attachment to membranes and association with caveolae. Mol. Cell. Biol. 15, 3507–3515.

Rodgers, W., Crise, B., Rose, J.K., 1994. Signals determining protein tyrosine kinase and glycosyl-phosphatidylinositol-anchored protein targeting to a glycolipid-enriched membrane fraction. Mol. Cell. Biol. 14, 5384–5391.

Roy, S., Luetterforst, R., Harding, A., Apolloni, A., Etheridge, M., Stang, E., Rolls, B., Hancock, J.F., Parton, R.G., 1999. Dominant-negative caveolin inhibits H-Ras function by disrupting cholesterol-rich plasma membrane domains. Nat. Cell Biol. 1, 98–105.

Scheiffele, P., Roth, M.G., Simons, K., 1997. Interaction of influenza virus haemagglutinin with sphingolipid-cholesterol membrane domains via its transmembrane domain. EMBO J. 16, 5501–5508.

Scheiffele, P., Rietveld, A., Wilk, T., Simons, K., 1999. Influenza viruses select ordered lipid domains during budding from the plasma membrane. J. Biol. Chem. 274, 2038–2044.

Schmitt, A.P., Lamb, R.A., 2004. Escaping from the cell: assembly and budding of negative-strand RNA viruses. Curr. Top. Microbiol. Immunol. 283, 145–196.

Schroeder, C., Ford, C.M., Wharton, S.A., Hay, A.J., 1994. Functional reconstitution in lipid vesicles of influenza virus M2 protein expressed by baculovirus: Evidence for proton transfer activity. J. Gen. Virol. 75, 3477–3484.

Schroeder, C., Heider, H., Moncke-Buchner, E., Lin, T.I., 2005. The influenza virus ion channel and maturation cofactor M2 is a cholesterol-binding protein. Eur. Biophys. J. 34, 52–66.

Sharma, P., Varma, R., Sarasij, R.C., Gousset, K., Krishnamoorthy, G., Rao, M., Mayor, S., 2004. Nanoscale organization of multiple GPI-anchored proteins in living cell membranes. Cell 116, 577–589.

Sheets, E.D., Holowka, D., Baird, B., 1999. Membrane organization in immunoglobulin E receptor signaling. Curr. Opin. Chem. Biol. 3, 95–99.

Simons, K., Ikonen, E., 1997. Functional rafts in cell membranes. Nature 387, 569–572.

Slot, J.W., Geuze, H.J., 1985. A new method for preparing gold probes for multiple-labeling cytochemistry. Eur. J. Cell Biol. 38, 87–93.

Suomalainen, M., 2002. Lipid rafts and assembly of enveloped viruses. Traffic 3, 705–709.

Takeda, M., Leser, G.P., Russell, C.J., Lamb, R.A., 2003. Influenza virus hemagglutinin concentrates in lipid raft microdomains for efficient viral fusion. Proc. Natl. Acad. Sci. U.S.A. 100, 14610–14617.

Varma, R., Mayor, S., 1998. GPI-anchored proteins are organized in submicron domains at the cell surface. Nature 394, 798–801.

Vincent, S., Gerlier, D., Manie, S.N., 2000. Measles virus assembly within membrane rafts. J. Virol. 74, 9911–9915.

Webb, Y., Hermida-Matsumoto, L., Resh, M.D., 2000. Inhibition of protein palmitoylation, raft localization, and T cell signaling by 2-bromopalmitate and polyunsaturated fatty acids. J. Biol. Chem. 275, 261–270.

Zebedee, S.L., Lamb, R.A., 1988. Influenza A virus M2 protein: monoclonal antibody restriction of virus growth and detection of M2 in virions. J. Virol. 62, 2762–2772.

Zhang, J., Pekosz, A., Lamb, R.A., 2000. Influenza virus assembly and lipid raft microdomains: a role for the cytoplasmic tails of the spike glycoproteins. J. Virol. 74, 4634–4644.